Supplementary Information

Supramolecular Control over the Variability of Color and Fluorescence in Low-Molecular-Weight Glass

Yunfei Zhang,[a] Changyong Cai,[a] Fenfang Li,[b] Xin Tan,[c] Qing Li,*[d] Xinlong Ni,*[e] Shengyi Dong*[a]

Y. Zhang, C. Cai, Prof. S. Dong

College of Chemistry and Chemical Engineering, Hunan University, Changsha 410082, China.

Prof. F. Li

College of Chemistry and Chemical Engineering, Central South University, Changsha 410083, China.

X. Tan

College of Life Science and Chemistry, Hunan University of Technology, Zhuzhou 412000, China.

Prof. Q. Li

College of Chemistry and Chemical Engineering, Guizhou University, Guiyang 550025, China.

Prof. X. Ni

College of Chemistry and Chemical Engineering, Hunan Normal University, Changsha 410081, China.

*To whom correspondence should be addressed.

E-mail: dongsy@hnu.edu.cn; liq@gzu.edu.cn; longni333@163.com

Table of Content

1. Materials and methods

Sodium sulphobutylether-β-cyclodextrin (**SC**), acid violet (**G1**), and acid blue (**G2**) were purchased from Shanghai Macklin Biochemical Technology Co., Ltd. Other solvents and materials were commercially obtained and used directly. NMR spectra were collected on a Bruker-AV400 (Germany) with TMS as the internal standard. Differential scanning calorimeter (DSC) measurements were obtained by a TAQ200 (American) with a heating rate of 10 °C from –80 to 200 °C in nitrogen atmosphere. Powder X-ray diffraction (PXRD) spectra were collected on an Ultima IV (Germany). Infrared (IR) spectra were collected on a Thermo Scientific Nicolet iS50 spectrometer (American). Dynamic thermomechanical analysis (DMA) was performed on a DMA 8000-PerkinElmer (American) using shear model. Nanoindentation results were obtained by an Anton Paar UNHT (Austria). Scanning electron microscopy (SEM) images were collected on a Sigma 300 (Germany). Atomic force microscope (AFM) images were collected on a Bruker (Germany). Small angle X-ray scattering (SAXS) was performed on a Xenocs Xeuss 3.0 (France). The adhesion strength measurements and tensile stress were performed on a HY-0580 Electronic tensile testing machine (China). Fluorescent emission spectra were recorded on an Edinburgh FS5 machine (Britain). The solid-state fluorescent emission spectra were measured on an Edinburgh FLS1000 machine (Britain). UV-Vis spectra were recorded on a SHIMADZU UV-2600 machine (Japan). The hot-pressing process was performed on a PCH-600C (China).

Computational details

Molecular dynamics simulations were conducted using GROMACS 5.1.1 to study the systems.[1] The GAFF force field, encompassing bonds, angles, dihedrals, and Lennard-Jones parameters, was applied to all components.[2] Partial charges were determined using the restrained electrostatic potential (RESP) method at the B3LYP/6-31+G (d,p) level. Electrostatic interactions were calculated with the particle mesh Ewald (PME) method. Equations of motion were solved using the leapfrog integration algorithm with a 2.0 fs time step. A 1.2 nm cutoff distance was employed for van der Waals and electrostatic interactions. The PME method utilized an interpolation order of 4 and a Fourier grid spacing of 0.10 nm.

The systems began with initial molecular structures containing 60 **WP** and 60 **SC** randomly distributed within a cubic box of 10 nm using PACKMO.[3,4] Following this, an energetic minimization process involving a steepest descent algorithm over 100,000 molecular simulation (MD) steps was conducted. Subsequently, both NVT and NPT ensembles were utilized, with temperature regulated by a V-rescale thermostat and pressure controlled through Parrinello−Rahman dynamics at 298.15 K and 1 atm. To ensure system stability, 2 ns simulations were carried out in both the NVT and NPT ensembles. This was followed by 5 ns simulations in the canonical ensemble for in-depth analysis, with trajectories recorded at intervals of 100 fs.

2. Synthesis of M and WP

M and **WP** were synthesized according to previously reported procedures.[5,6]

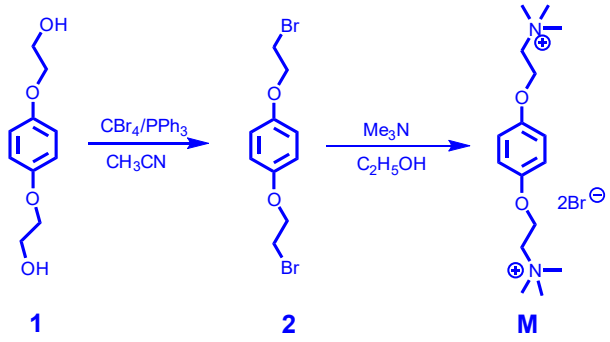

Scheme S1. Synthesis of compound **M**.

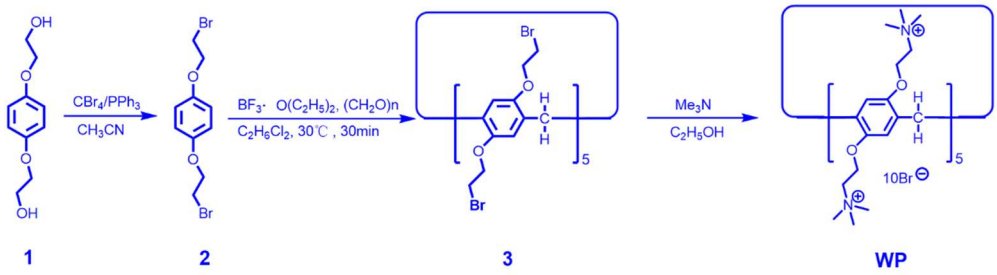

Scheme S2. Synthesis of compound **WP**.

Preparation of WP-SC

SC (2.0 mmol, 4.4840 g), **WP** (0.2 mmol, 0.5733 g) and water were mixed in a beaker, then the mixture was evaporated in an oven at 80 °C until constant weight. Supramolecular transparent material **WP-SC** was obtained by hot-pressing. The hot-pressing temperature is 80 °C and the pressure is 10 MPa.

Unless otherwise noted, the ratio of **SC** and **WP** in this study is molar ratio.

3. The property of WP-SC

Table S1. Essential information of **WP-SC** (1: 10).

	Density (g/cm^3)	Refractivity
WP-SC	1.21	1.501

4. Atomic force microscopy (AFM)

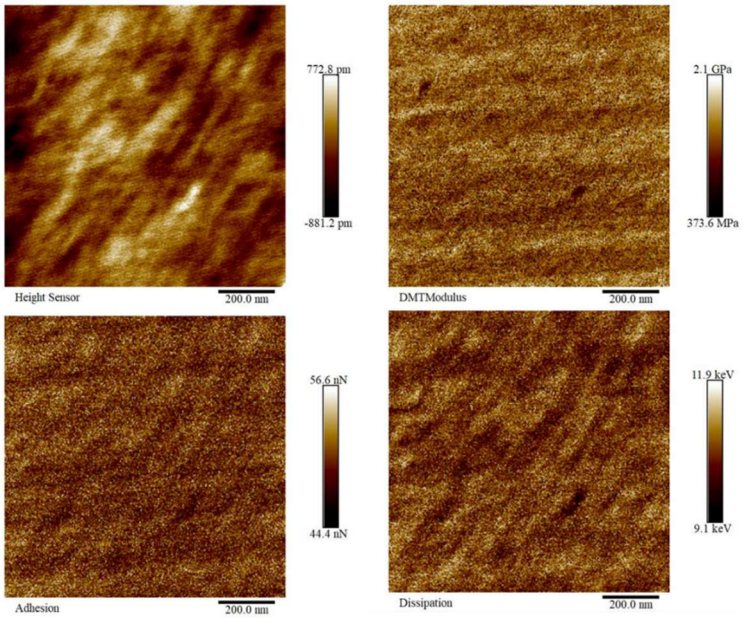

Figure S1. AFM images of **WP-SC**.

5. Scanning electron microscopy (SEM)

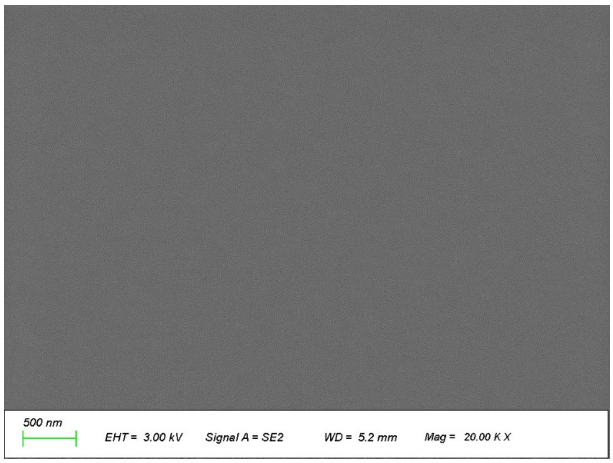

Figure S2. SEM image of **WP-SC**.

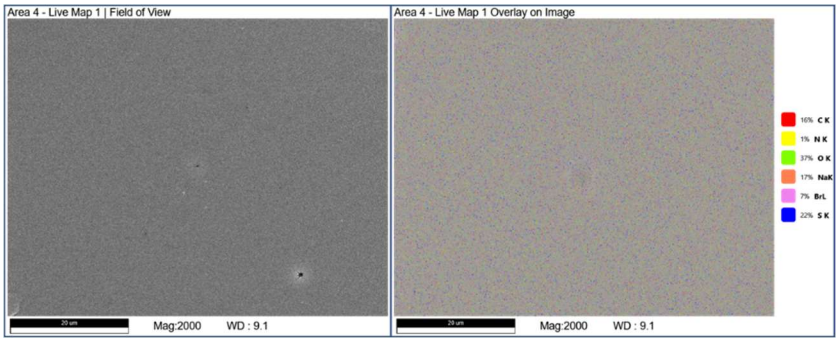

Figure S3. EDS (mapping) images of **WP-SC**.

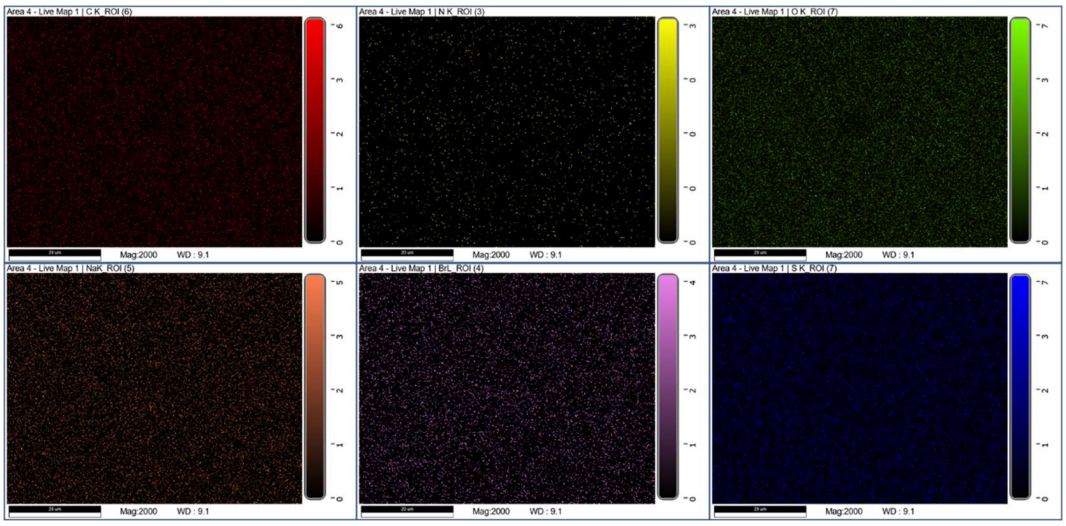

Figure S4. EDS (mapping) images (C, N, O, S, Br and Na) of **WP-SC**.

6. NMR spectra

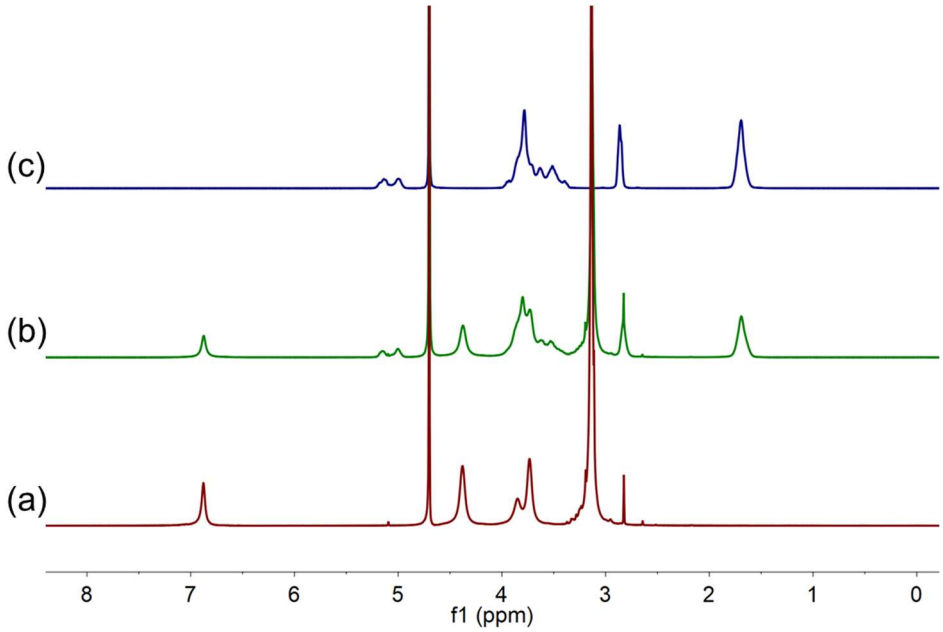

Figure S5. ^{1}H NMR spectra (400 MHz, D_2O, room temperature): (a) **WP**; (b) **WP-SC**; and (c) **SC**.

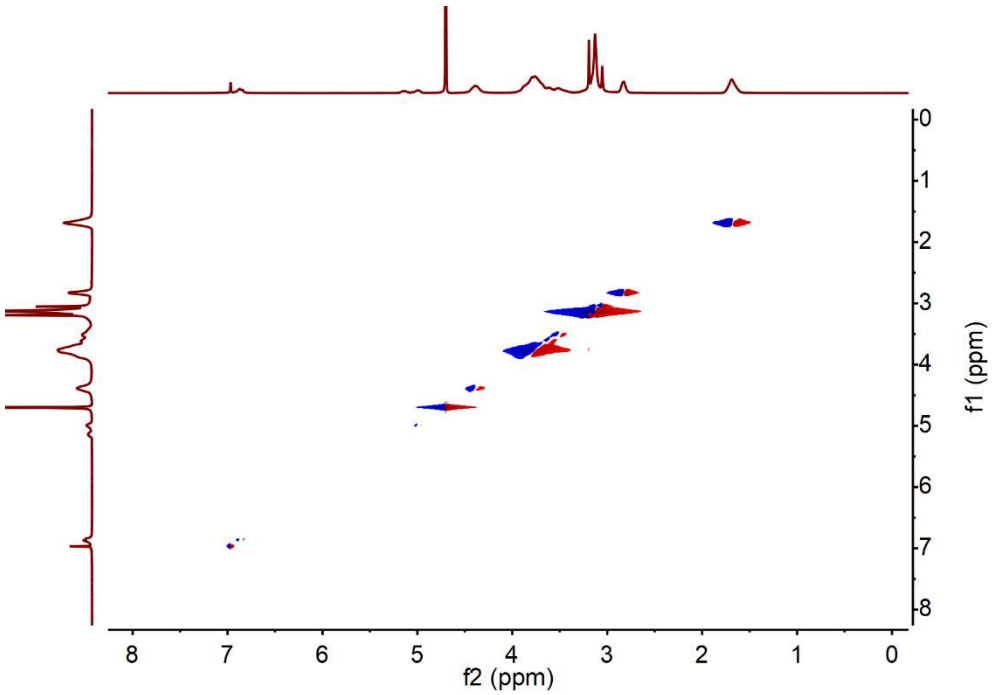

Figure S6. 2D NOESY spectra (400 MHz, D_2O, room temperature) of **WP-SC**.

7. Powder X-Ray diffraction (PXRD) patterns

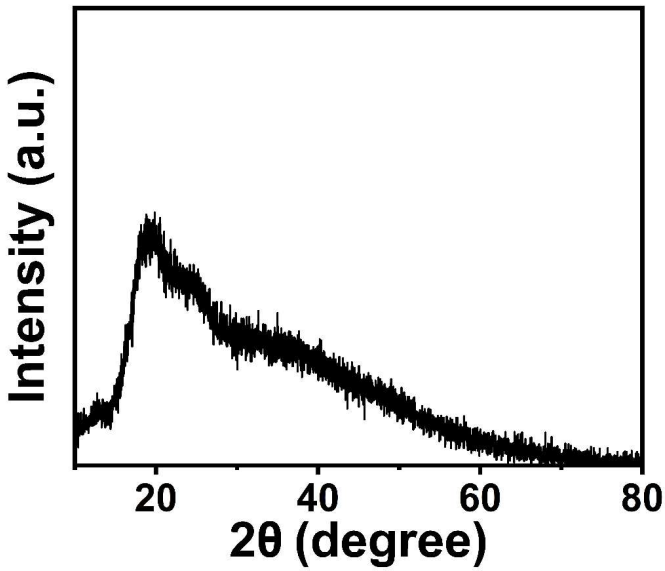

Figure S7. PXRD spectrum of **WP-SC**.

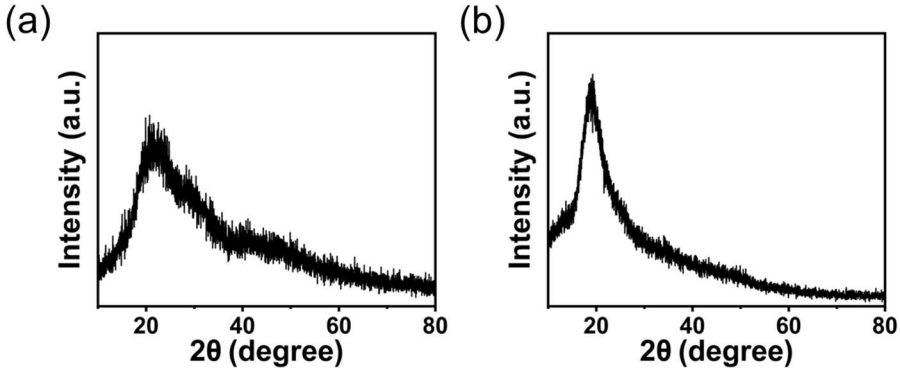

Figure S8. PXRD spectra: (a) **WP** and (b) **SC**.

8. Small-angle X-ray scattering (SAXS)

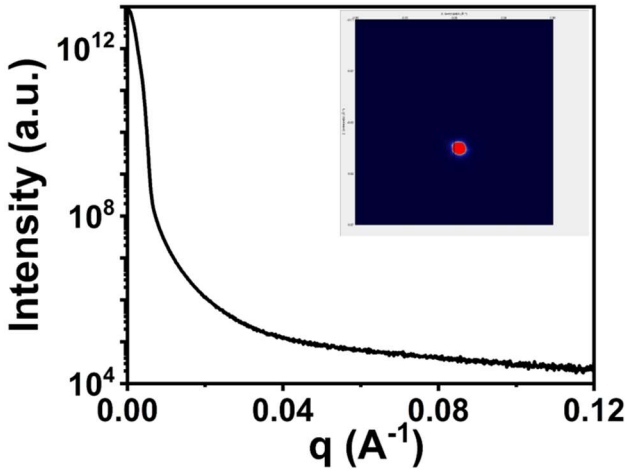

Figure S9. SAXS spectrum of **WP-SC**.

9. Theoretical calculation

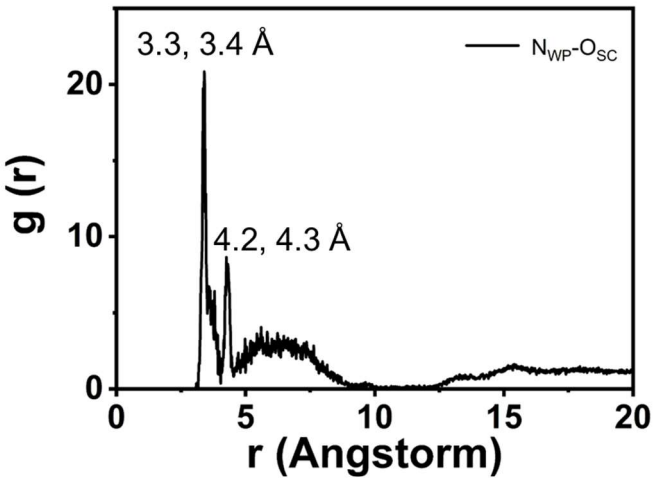

Figure S10. RDF of N_{WP}-O_{SC} for the mixture of **WP** and **SC**.

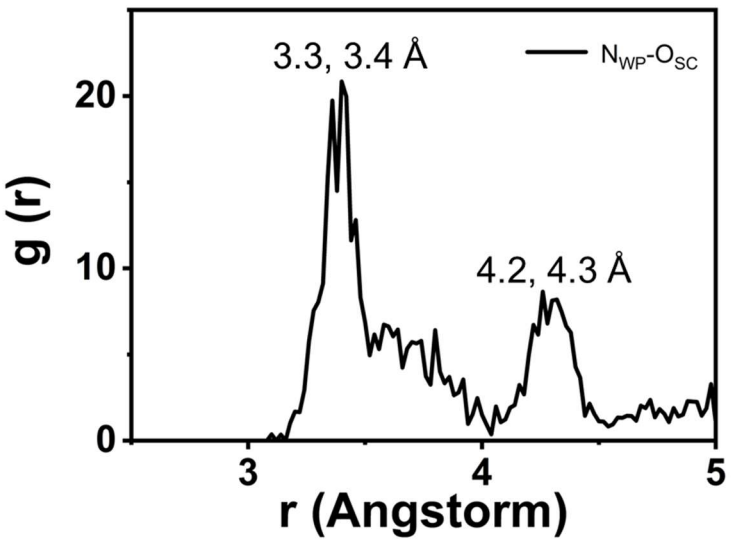

Figure S11. The partial RDF of N_{WP}-O_{SC} for the mixture of **WP** and **SC** below 5Å.

10. The mechanism of WP-SC glass formation

According the experimental and theoretical investigation, possible glass formation mechanism and process were provided:

In the solution state, **WP** and **SC** molecules exist as monomers because of the strong solvation effect of water molecules (Figure S5,6). Upon heating, a large amounts of water molecules are removed from **WP-SC**, thus strongly enhancing the intermolecular interactions between **WP-SC**, which include hydrogen bonds and electrostatic interactions. Considering that there are multiple molecular recognition sites in both **WP** and **SC**, it is possible for the formation of three-dimensional networks in **WP-SC**. Simulation results showed that **WP-SC** has a high cohesive energy density at 8.38 × 10^5 kJ/mol, displaying its high electrostatic interaction and hydrogen bond density. During the water-evaporation process, a rapid transition from a diluted solution to a solid was recorded, indicating that the crystallization behaves of **WP** and **SC** were strongly suppressed. Therefore, the obtained **WP-SC** is an amorphous material instead of as a crystallized mixture, demonstrating that **WP-SC** is long-range disordered and isotropic (Figure S7-9). Simulations and SEM mapping clearly showed that **WP** and **SC** were uniformly dispersed in **WP-SC** (Figure S3,4). In addition, DSC data shows that the glass transition temperature of **WP-SC** is 54 °C, indicating that it is a typical

amorphous material (Figure S20).

Although **WP-SC** is isotropic macroscopically, it does not mean there is no short-range ordered structure in it. Due to the directionality of hydrogen bonding, there are relatively ordered structures in **WP-SC**, when the scale is below 10 Å. Herein, we applied RDF calculation to study the short-range order. As shown in Figure S10,11, no peaks were found when the distance is above 10 Å. The distinguished peaks at 3.3, 3.4, 4.2 and 4.3 Å were observed.

11. Nanoindentation

Table S2. Hardness and reduced modulus of **WP-SC** sample by nanoindentation.

	Reduced modulus (GPa)	Hardness (GPa)
Average	2.2559 ± 0.1446	0.0667 ± 0.0087

12. Mechanical properties testing

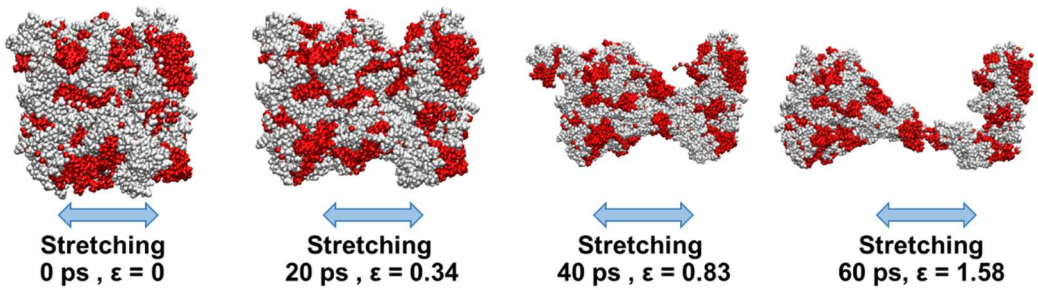

Figure S12. The structure evolution of **WP-SC** during the elongation process (white: **SC**, red: **WP**).

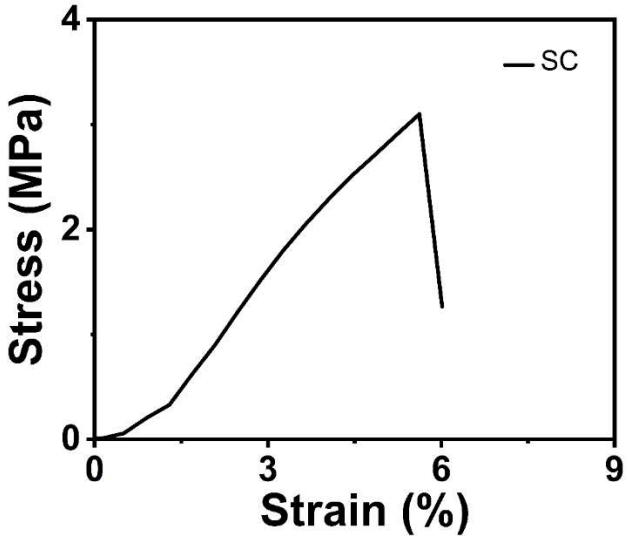

Figure S13. Stress-strain curve of **SC**.

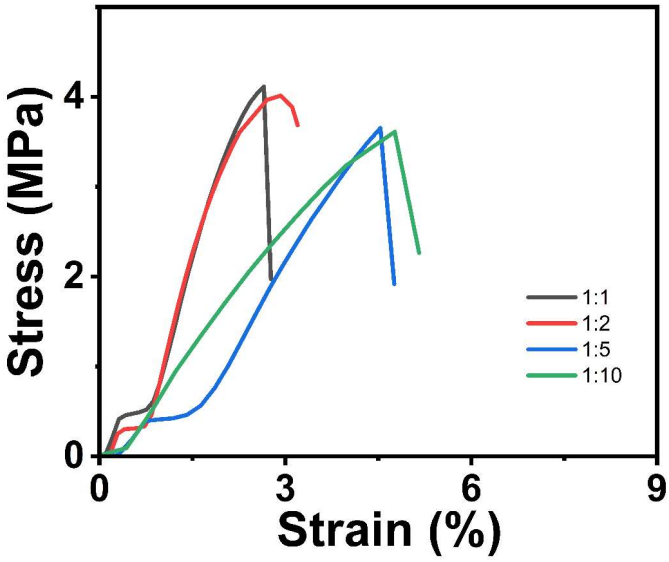

Figure S14. The stress-strain curves of **WP-SC** after 20 days of storage (25 °C, 50% RH).

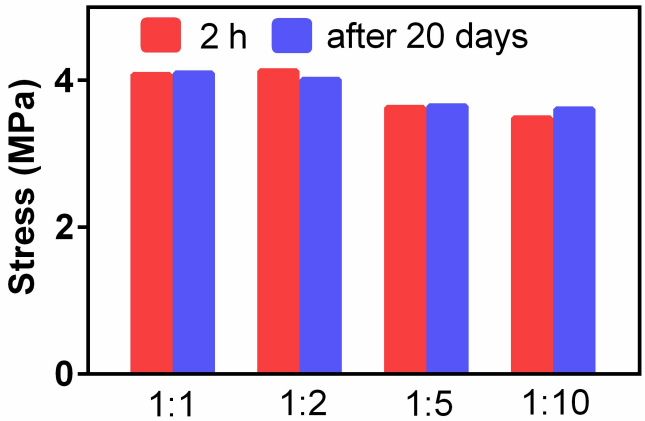

Figure S15. The stress of **WP-SC** at different times (2 h and 20 days, 25 °C, 50% RH).

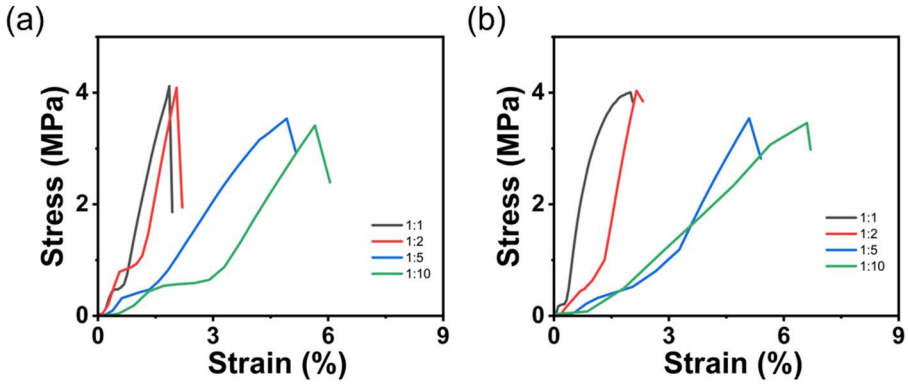

Figure S16. The stress-strain curves of **WP-SC** with different molar ratio under different humidity for 2 h: (a) 70% RH and (b) 90% RH.

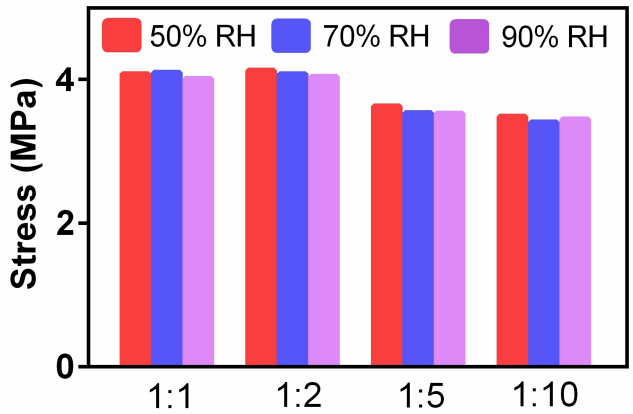

Figure S17. The stress of **WP-SC** with different molar ratio under different humidity for 2 h.

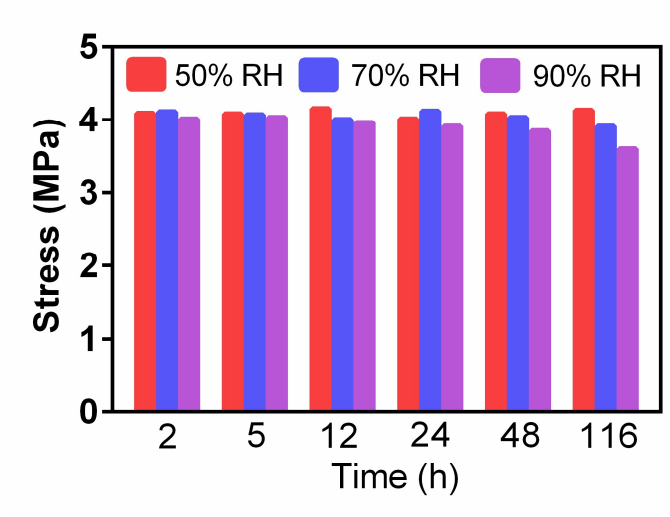

Figure S18. The stress of **WP-SC** (**WP**: **SC** = 1: 1) under different humidity levels for different times.

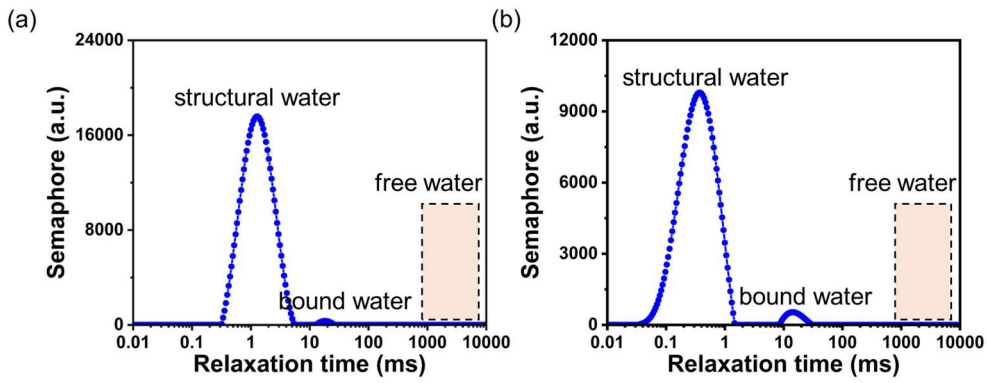

Figure S19. The low-field NMR spectra of **WP-SC** under different humidity for 24 h: (a) 50% RH and (b) 90% RH.

The low-field NMR spectra of **WP-SC** samples with different incubation time in humid environment showed that water molecules existed as structural/bound water. No free water (bulk water cluster, with relaxation time above 1000 ms) was recorded. These observations indicate that a small amount of water molecules parcipate in the formation of non-covalent supramolecular networks in **WP-SC** by hydrogen bonding.

13. Differential scanning calorimeter (DSC)

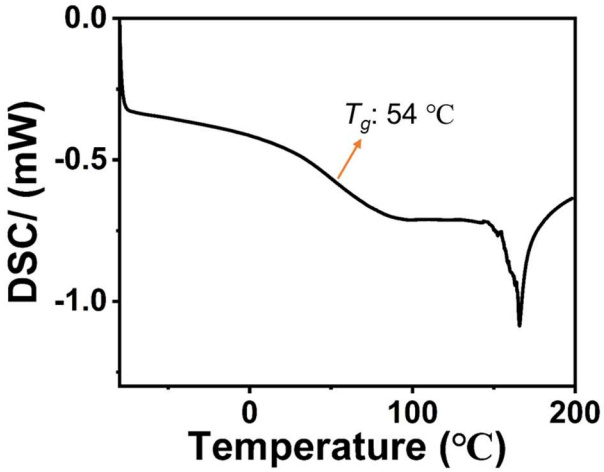

Figure S20. DSC spectrum of **WP-SC**.

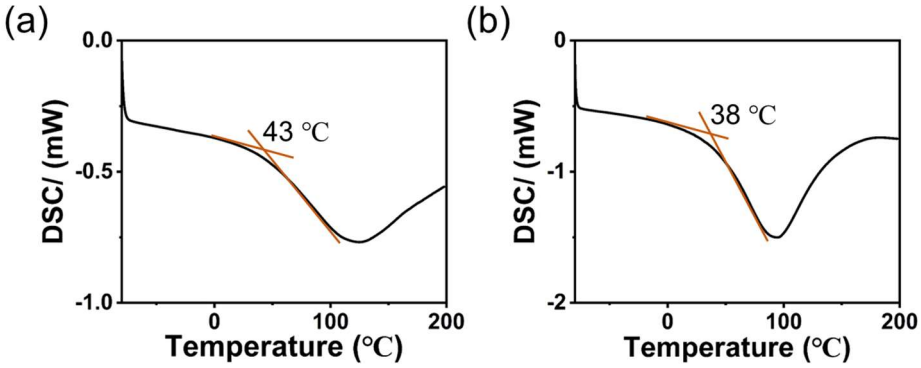

Figure S21. DSC spectra: (a) **WP** and (b) **SC**.

14. Dynamic thermomechanical analysis (DMA)

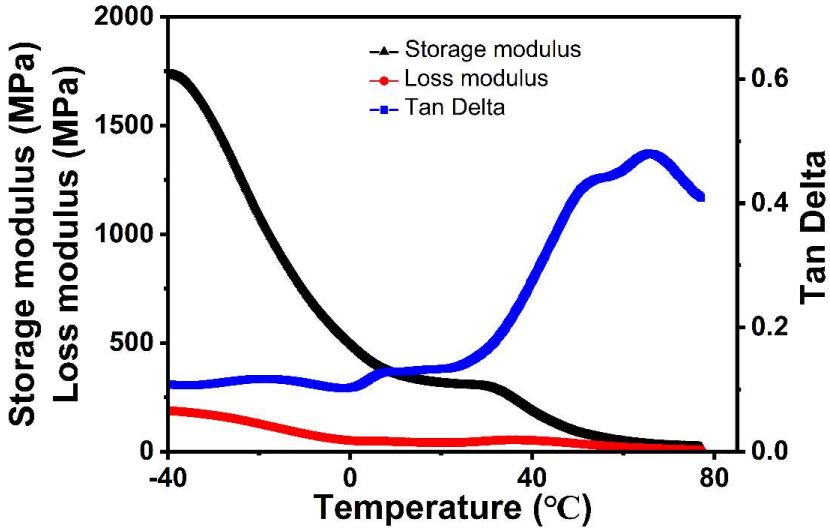

Figure S22. DMA test of **WP-SC**.

15. Thermogravimetric analysis (TGA)

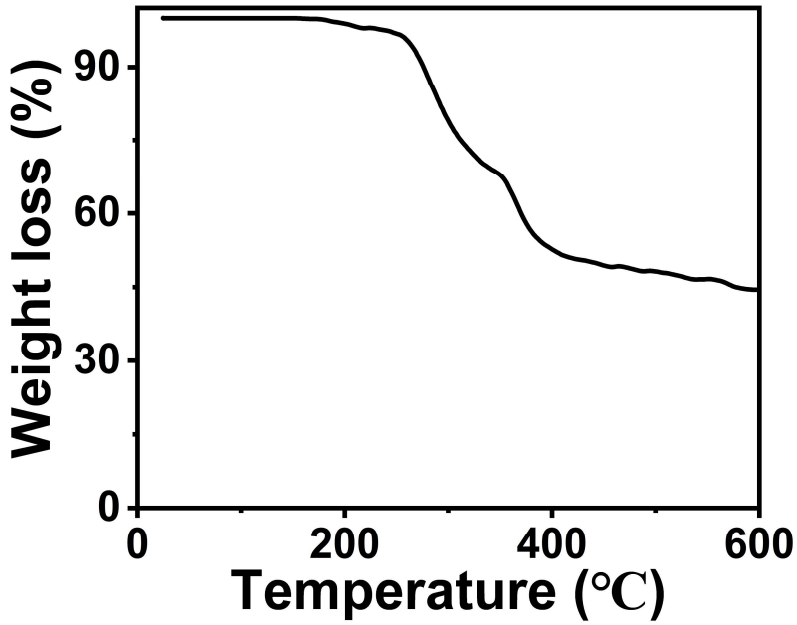

Figure S23. TGA spectrum of **WP-SC**.

16. UV-vis spectra

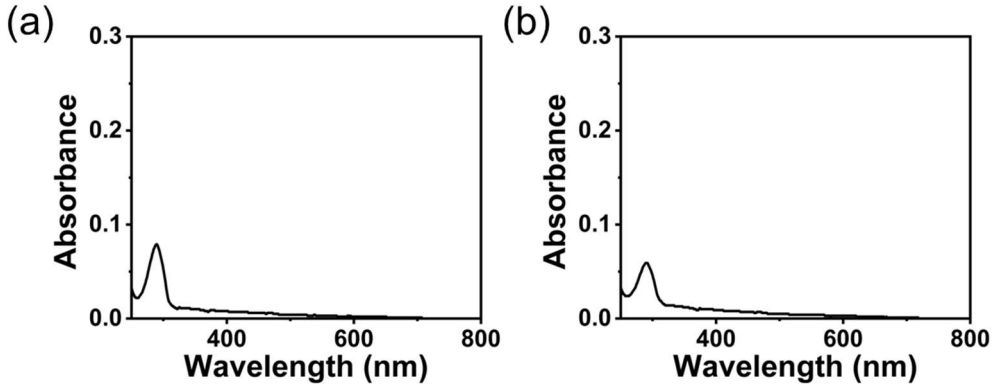

Figure S24. UV-vis spectra (1×10^{-5} mol/L): (a) **WP** and (b) **WP-SC**.

17. Color tuning

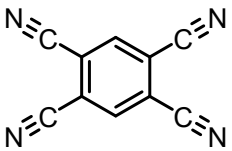

1,2,4,5-Tetracyanobenzene (**G3**)

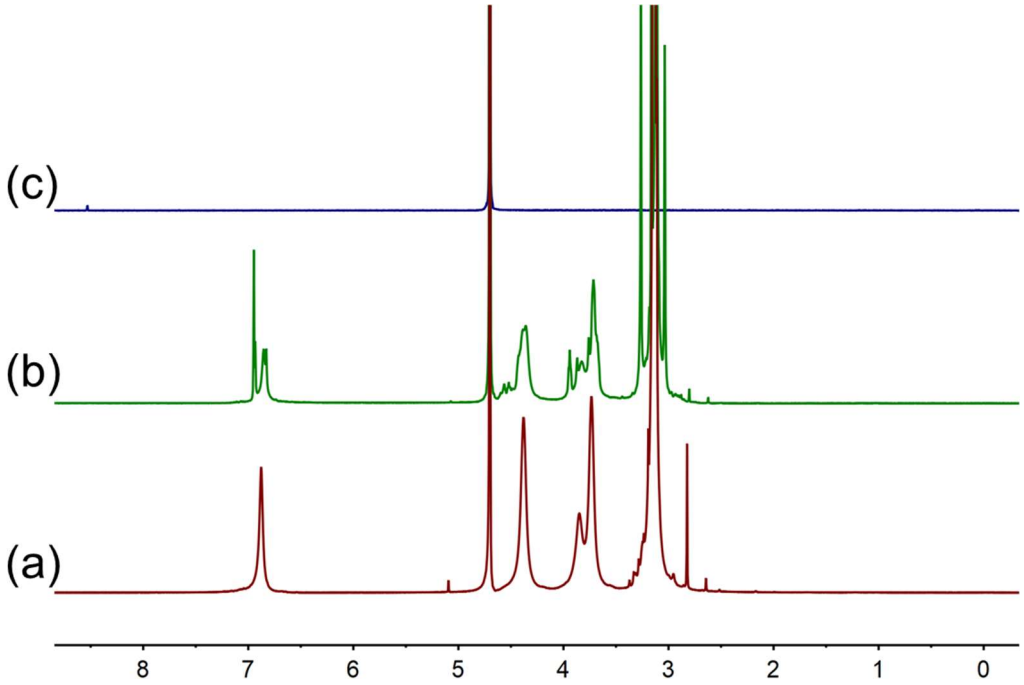

Figure S25. ^{1}H NMR spectra (400 MHz, D_2O, room temperature): (a) **WP**; (b) **WP-G3**; and (c) **G3**.

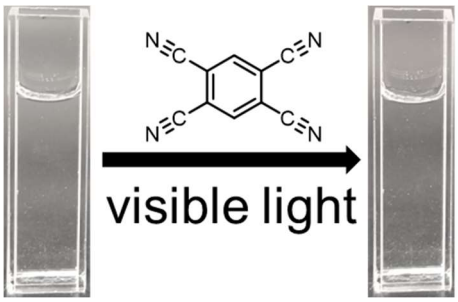

Figure S26. SC-G3 solution under visible light.

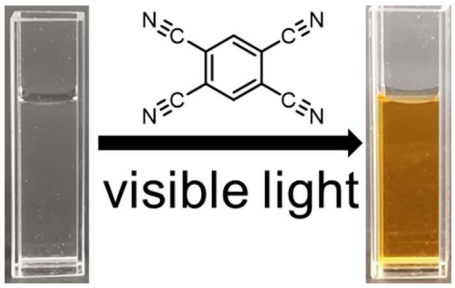

Figure S27. WP-SC-G3 solution under visible light.

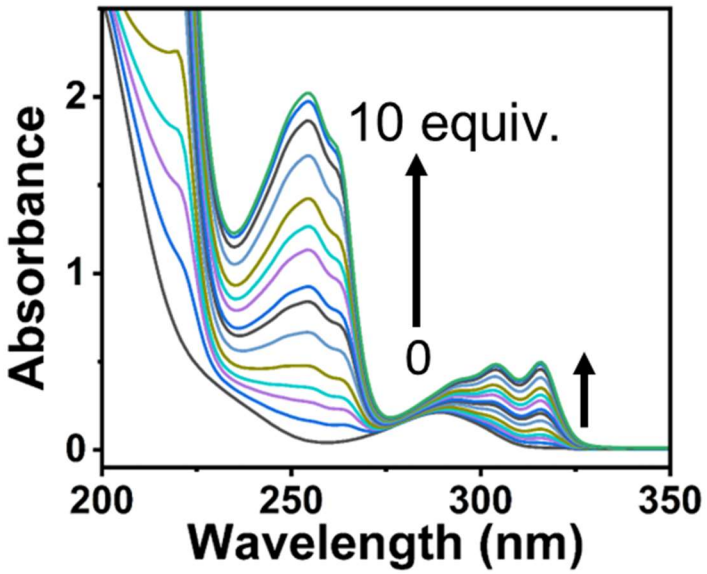

Figure S28. UV titration experiments of **WP** solution (1×10^{-5} mol/L) upon the addition of **G3**.

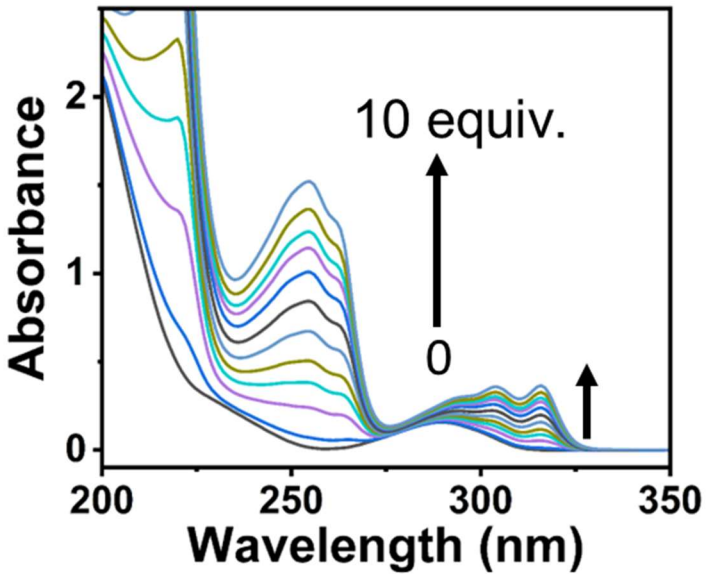

Figure S29. UV titration experiments of **WP-SC** solution (1×10^{-5} mol/L) upon the addition of **G3**.

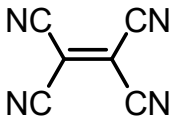

Tetracyanoethylene (**G4**)

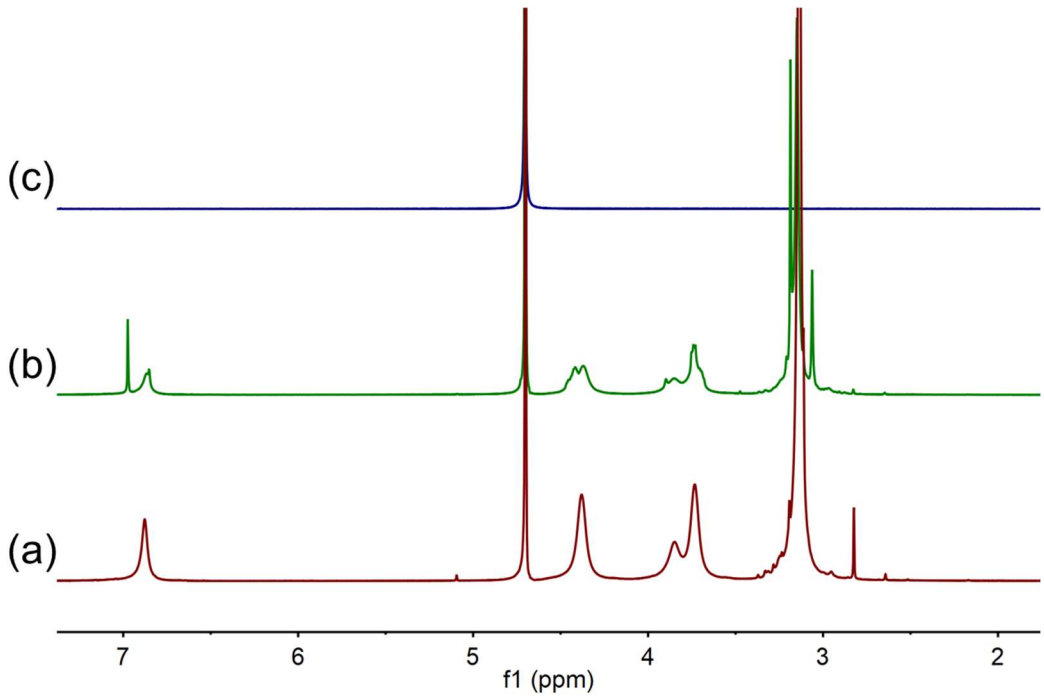

Figure S30. ^{1}H NMR spectra (400 MHz, D_2O, room temperature): (a) **WP**; (b) **WP-G4**; and (c) **G4**.

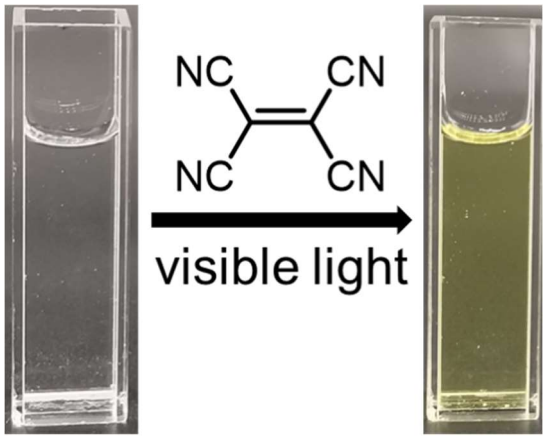

Figure S31. WP-G4 solution under visible light.

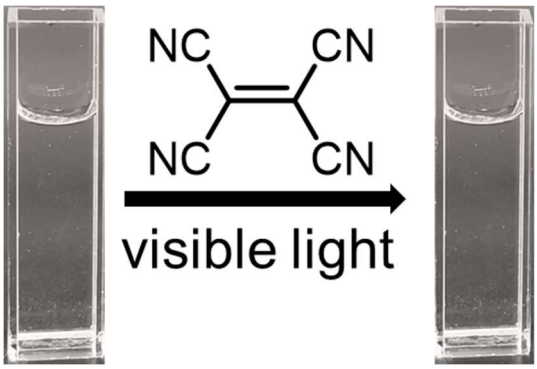

Figure S32. SC-G4 solution under visible light.

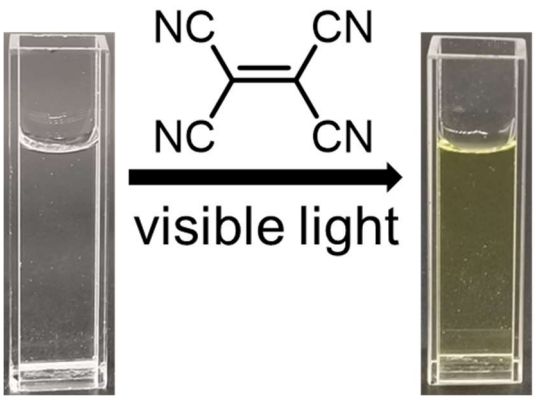

Figure S33. WP-SC-G4 solution under visible light.

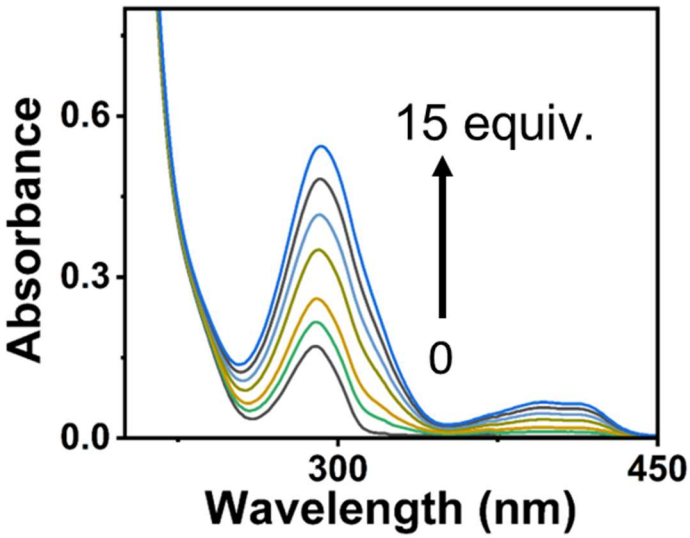

Figure S34. UV titration experiments of **WP** solution (1×10^{-5} mol/L) upon the addition of **G4**.

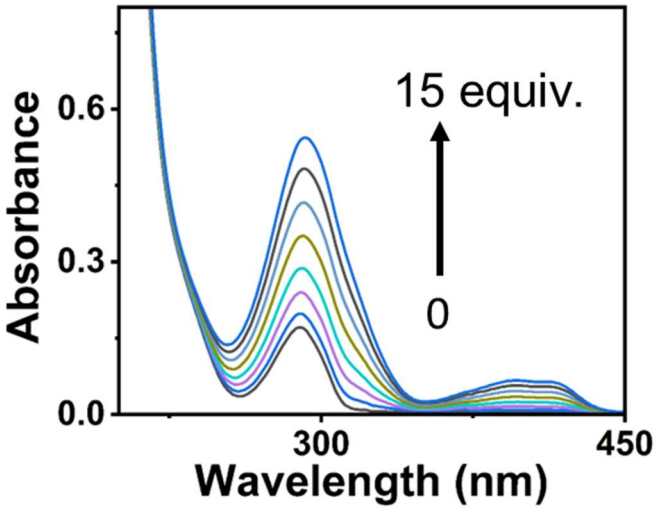

Figure S35. UV titration experiments of **WP-SC** solution (1×10^{-5} mol/L) upon the addition of **G4**.

As shown in Figure S25-35, after adding **G3** into the **WP** solution, the color transformation from colorless to brown for the solution of **WP** with **G3**, as well as the absorption peak at 290 nm showed a red shift. In addition, as shown in Figure S25, in D_2O, after the addition of **G3** to a solution of **WP**, the signals of **G3** shifted downfield after complexation. These results indicated that there charge-transfer interaction between **WP** and **G3**/**G4**.

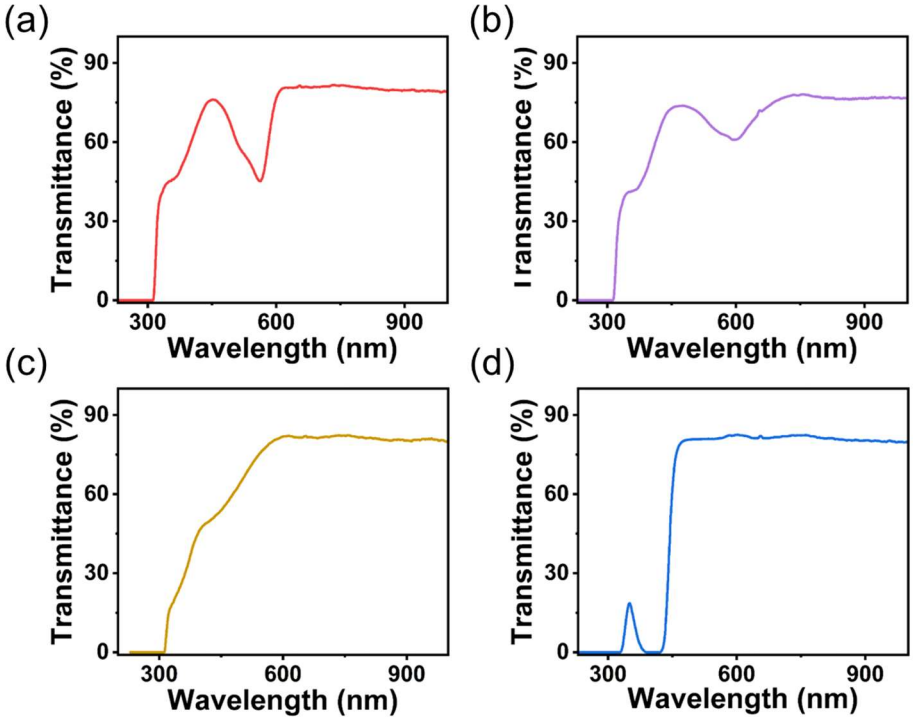

Figure S36. Transmittances: (a) **WP-SC-G1**; (b) **WP-SC-G2**; (c) **WP-SC-G3**; and (d) **WP-SC-G4**.

18. Fluorescence regulation

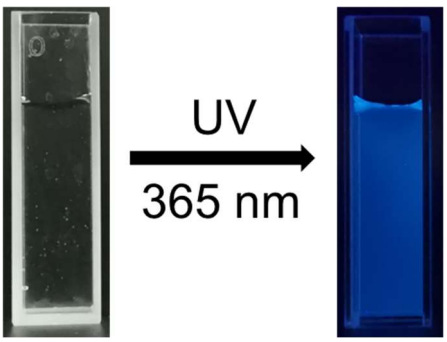

Figure S37. WP-SC solution under UV irradiation (365 nm).

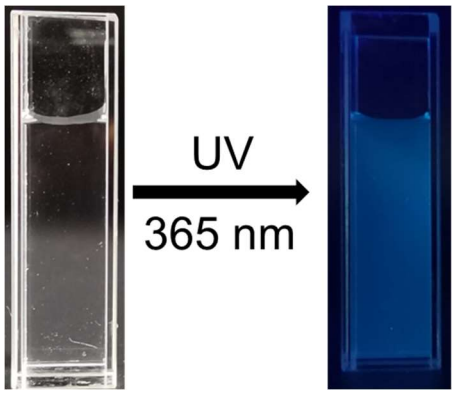

Figure S38. WP solution under UV irradiation (365 nm).

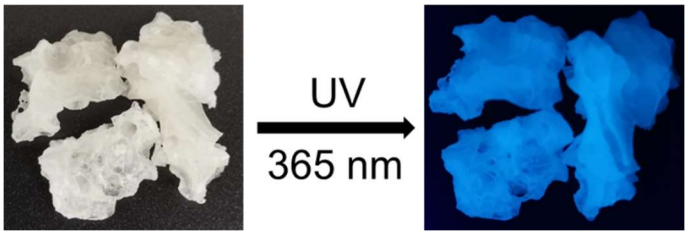

Figure S39. WP solid under UV irradiation (365 nm).

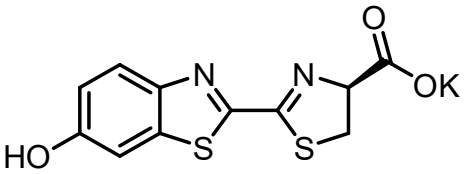

D-Luciferin potassium salt (**G5**)

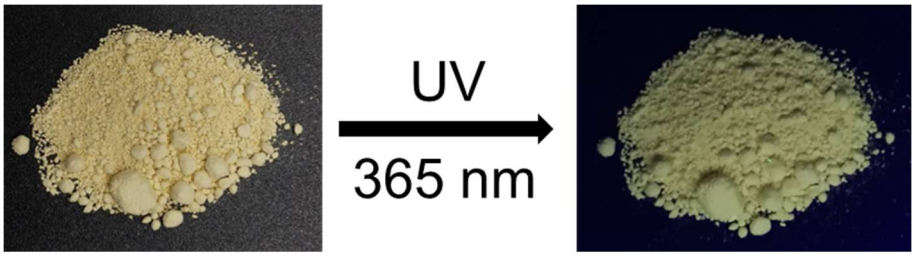

Figure S40. G5 solid under UV irradiation (365 nm).

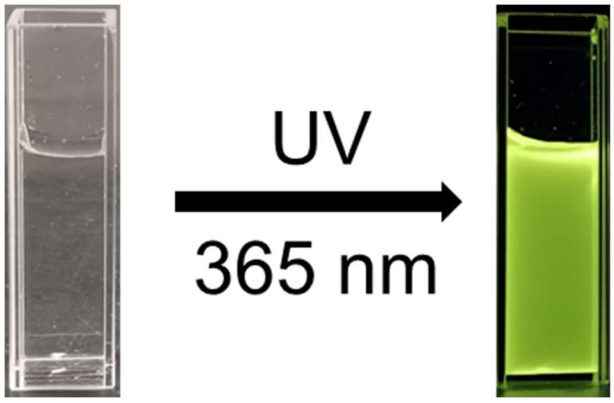

Figure S41. G5 solution under UV irradiation (365 nm).

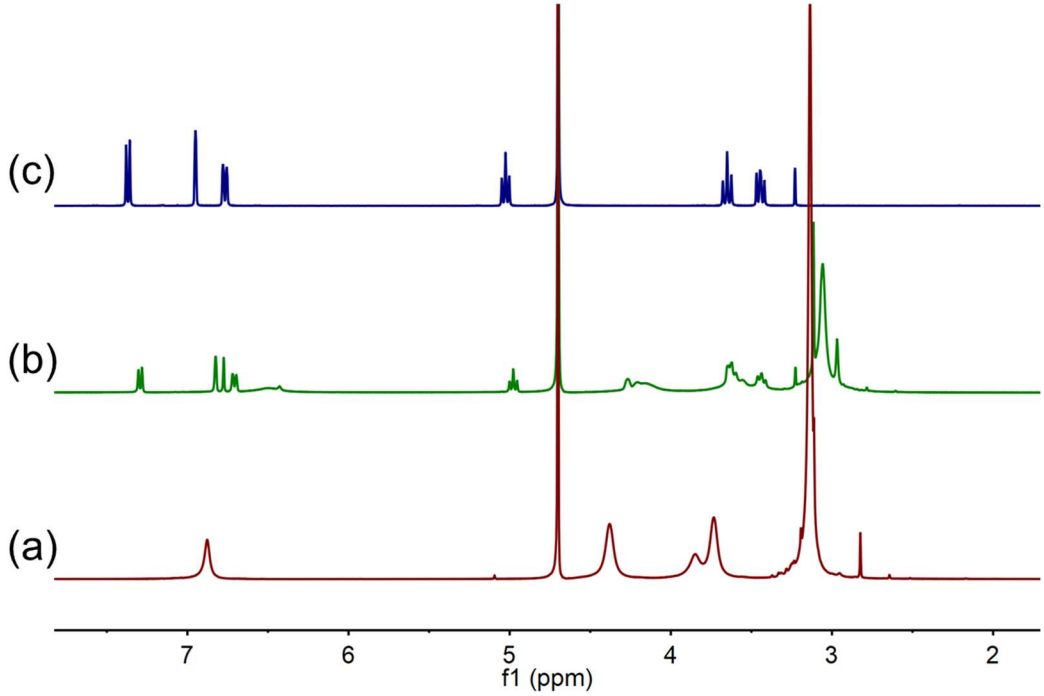

Figure S42. ^{1}H NMR spectra (400 MHz, D_2O, room temperature): (a) **WP**; (b) **WP-G5**; and (c) **G5**.

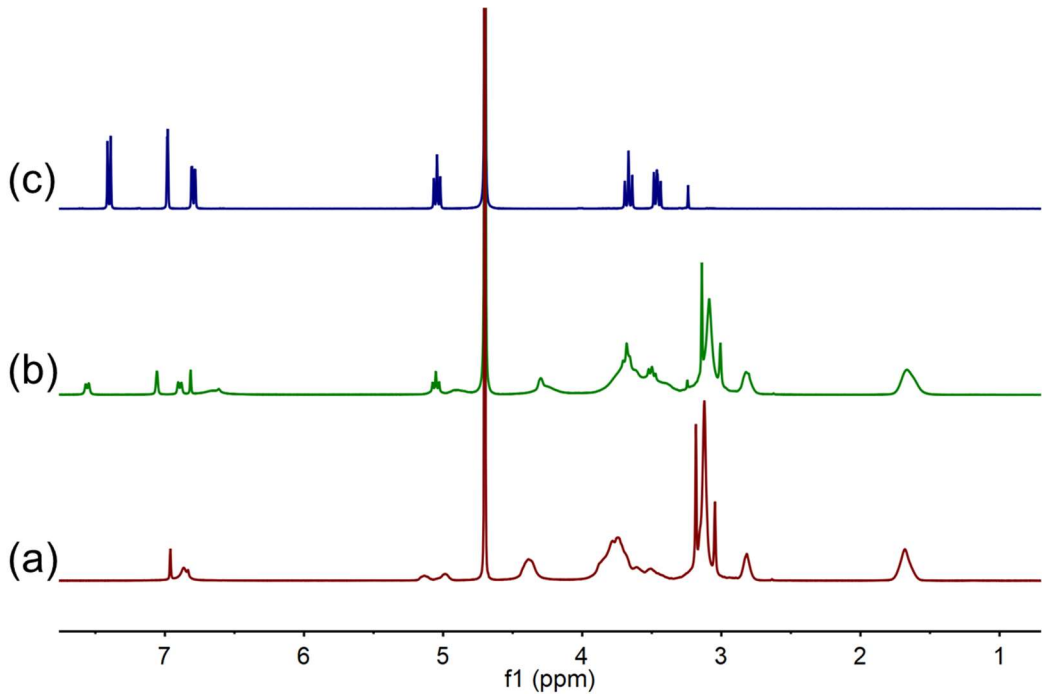

Figure S43. ^{1}H NMR spectra (400 MHz, D_2O, room temperature): (a) **WP-SC**, (b) **WP-SC-G5**, and (c) **G5**.

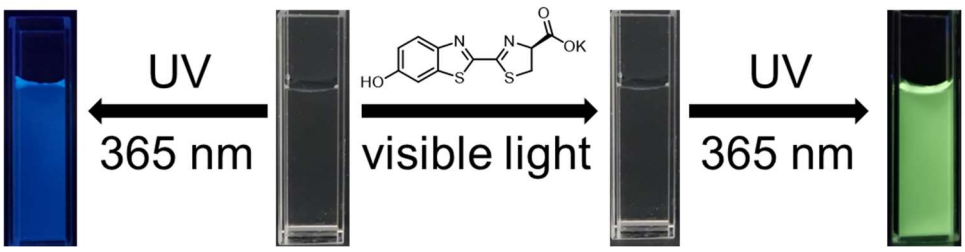

Figure S44. WP-SC solution upon the addition of **G5** under visible light and UV irradiation (365 nm).

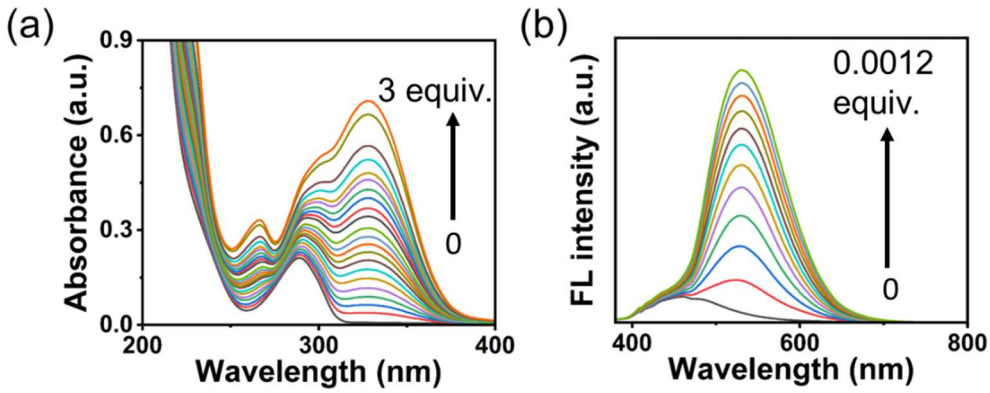

Figure S45. Fluorescence emission and UV spectra: (a) UV titration experiments of **WP** solution (1×10^{-5} mol/L) upon the addition of **G5**; (b) fluorescence titration experiments of **WP** solution (1×10^{-2} mol/L) upon the addition of **G5** (excitation

wavelength: 365 nm).

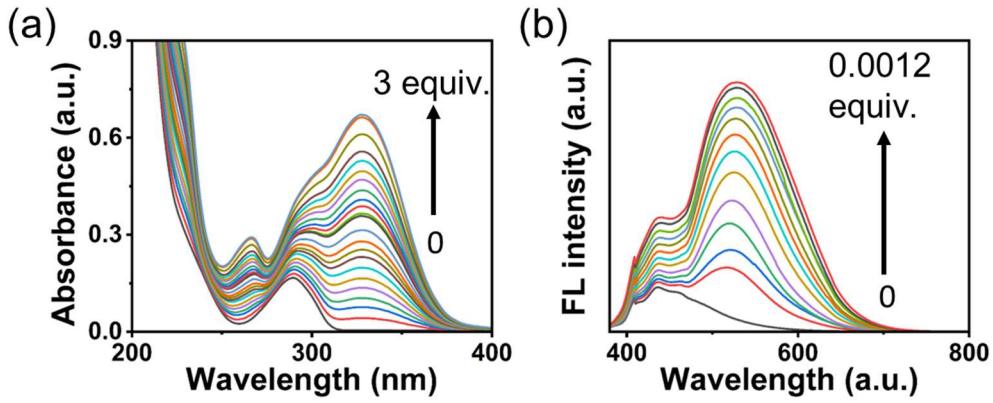

Figure S46. Fluorescence emission and UV spectra: (a) UV titration experiments of **WP-SC** solution (1×10^{-5} mol/L) upon the addition of **G5**; (b) fluorescence titration experiments of **WP-SC** solution (1×10^{-2} mol/L) upon the addition of **G5** (excitation wavelength: 365 nm).

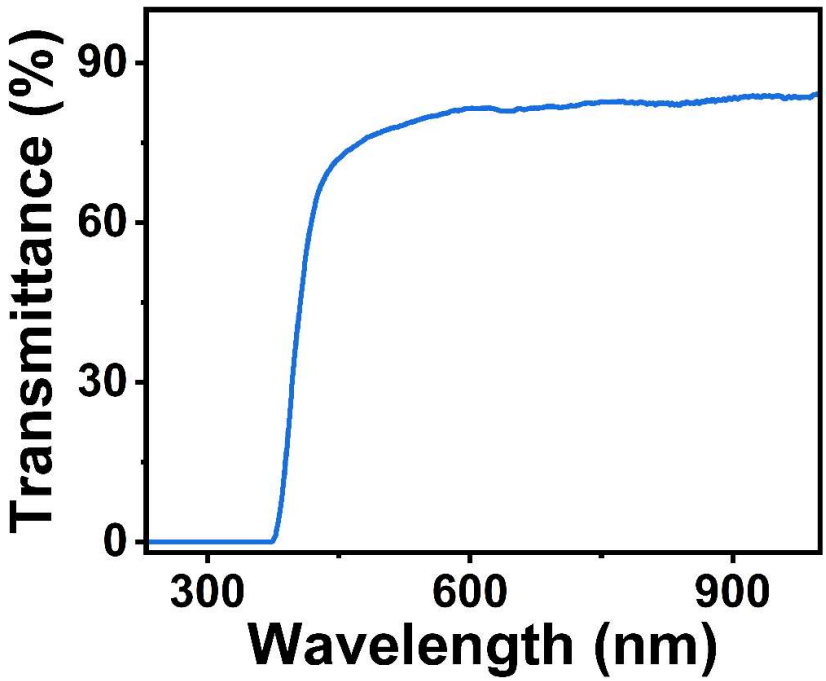

Figure S47. Transmittance of **WP-SC-G5**.

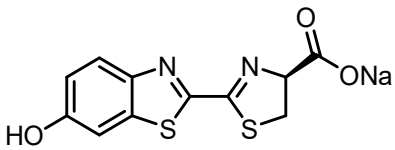

D-Luorescein sodium salt (**G6**)

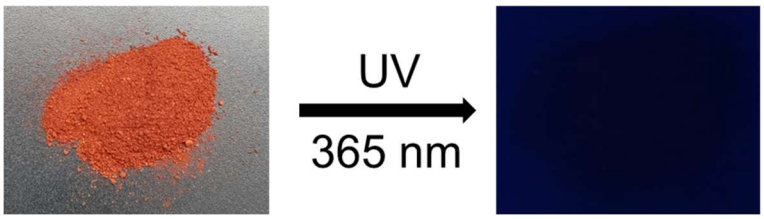

Figure S48. G6 solid under UV irradiation (365 nm).

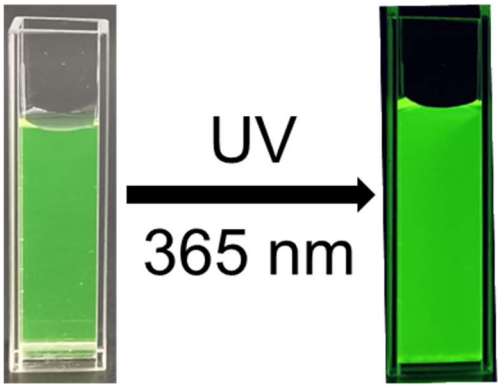

Figure S49. G6 solution under UV irradiation (365 nm).

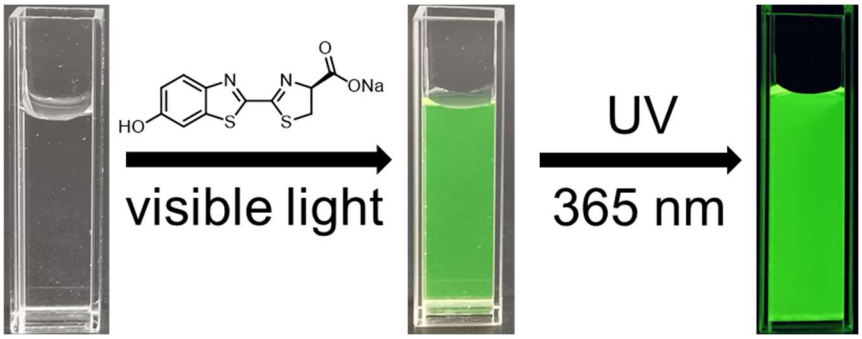

Figure S50. WP-SC solution upon the addition of **G6** under visible light and UV irradiation (365 nm).

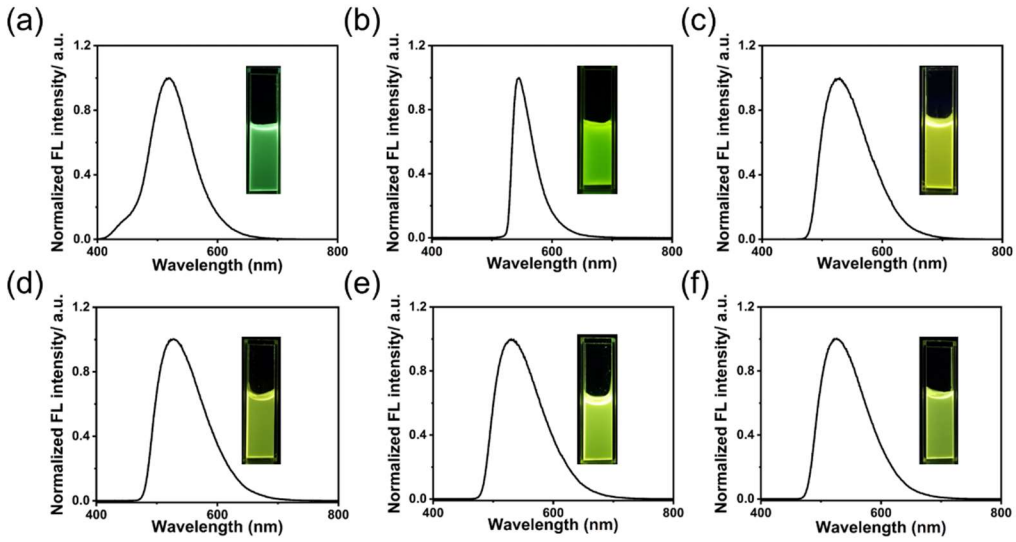

Figure S51. Fluorescence emission spectra in solution (excitation wavelength: 365 nm): (a) **WP-SC-G5**; (b) **WP-SC-G6**; and (c-f) **WP-SC-CB**[8]/**G**7 system.[7]

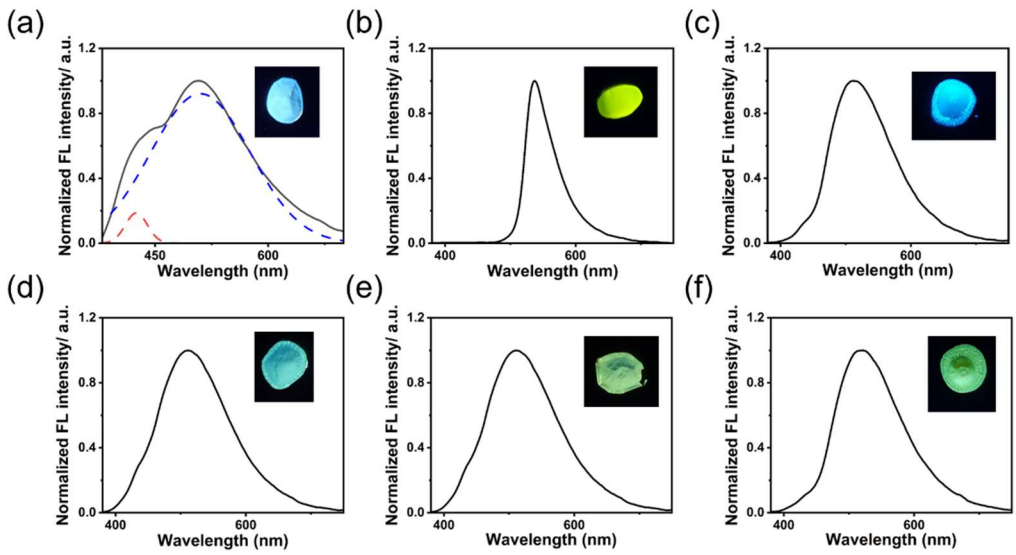

Figure S52. Fluorescence emission spectra in solid (excitation wavelength: 365 nm): (a) **WP-SC-G5**; (b) **WP-SC-G6**; and (c-f) **WP-SC-CB**[8]/**G**7 system.[7]

19. References

[1] D. Van der Spoel, E. Lindahl, B. Hess, G. Groenhof, A. E. Mark, and H. J. C. Berendsen. *J. Comput. Chem.*, 2005, **26**, 1701−1718.

[2] J. M. Wang, et al. *J. Comput. Chem.*, 2004, **25**, 1157−1174.

[3] J. M. Martinez and L. *J. Comput. Chem.*, 2003, **24**, 819−825.

[4] L. Martinez, et al. PACKMOL: *J. Comput. Chem.*, 2009, **30**, 2157−2164.

[5] Y. J. Ma, X. F. Ji, F. Xiang, X. D. Chi, C. Y. Han, J. M. He, Z. Abliz, W. X. Chen, and F. Huang. *Chem. Commun.*, 2011, **47**, 12340–12342.

[6] B. Hua, L. Shao, G. Yu, and F. Huang. *Chem. Commun.*, 2016, **52**, 10016–10019.

[7] X.-L. Ni, S. Chen, Y. Yang, and Z. Tao. *J. Am. Chem. Soc.*, 2016, **138**, 6177−6183.